


Metal Transition in Sodium–Ammonia Nanodroplets

Journal Article**Author(s):**

Hartweg, Sebastian; West, Adam H.C.; Yoder, Bruce L.; [Signorell, Ruth](#) 

Publication date:

2016-09-26

Permanent link:

<https://doi.org/10.3929/ethz-b-000121397>

Rights / license:

[In Copyright - Non-Commercial Use Permitted](#)

Originally published in:

Angewandte Chemie 55(40), <https://doi.org/10.1002/anie.201604282>

Funding acknowledgement:

159205 - Interaction of Light with Ultrafine Aerosol Particles II (SNF)

Supporting Information

Metal Transition in Sodium-Ammonia Nanodroplets

*Sebastian Hartweg, Adam H. C. West, Bruce L. Yoder, and Ruth Signorell**

Contents

S1	Cluster Size Distribution, Determination of the average MPM, Cluster Temperature.....	3
S1.1	Cluster Size Distribution	
S1.2	Determination of the average MPM	
S1.3	Cluster Temperature	
S2	Photoelectron Images.....	7
S3	Ab initio Calculations.....	8
S4	Photoelectron Spectra and Size Distributions of Small Na-Ammonia Clusters.....	9
S5	Photoelectron Spectra and Size Distributions of Na-Dimethyl Ether Clusters.....	11
S6	References.....	14

S1 Cluster Size Distribution, Determination of the average MPM; Cluster Temperature

S1.1 Cluster Size Distribution

The cluster size distributions are obtained from mass spectra. Different Na-doping levels are realized by changing the temperature in the Na pickup cell, thus changing the Na partial pressure. Details are reported in refs.^[1] Figure S1 shows the mass spectra that correspond to the photoelectron spectra (PES) in Figure 1 in the main text.

Small bare Na_j clusters ($j \leq 17$) are visible in mass spectra for MPMs > 4.4 . In Figure S1, bare Na clusters up to $j = 17$ are labelled with arrows in the 8.8 MPM mass spectrum. It is important to note that these bare Na clusters cannot contribute to the band B_{solV} in the PES at 8.8 MPM in Figure 1 in the main text because their binding energies (eBEs) are too high. Bare Na_j clusters with $j \leq 22$ have eBEs above ~ 3.7 eV^[2] and for $j \leq 14$ photoelectron threshold (PET) values above 3.5 eV.^[3] We note that even the PETs of Na clusters with $j > 1000$ and of Na-bulk lie above ~ 2.7 eV.^[4] Furthermore, bare Na clusters are also observed in the mass spectra of Na-dimethyl ether clusters containing > 6.2 MPM in Figure S9 (Section S5), with no significant influence on the position and shape of B_{solV} (Figure S7).

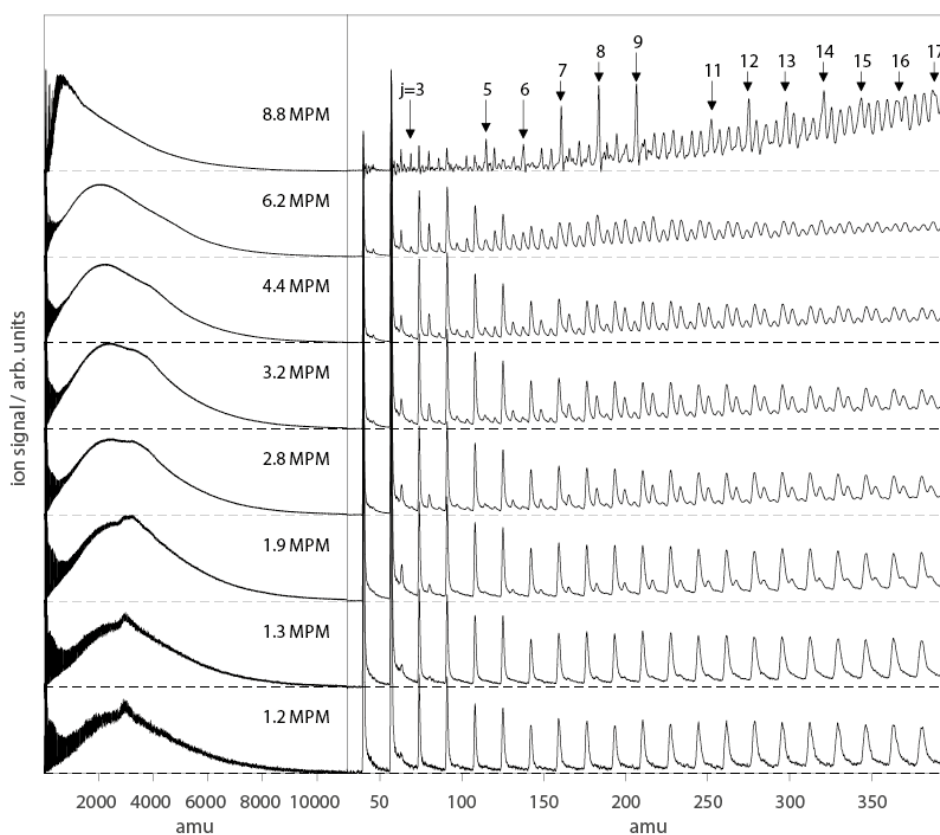


Figure S1: Mass spectra of $\text{Na}_m(\text{NH}_3)_n$ clusters. Left panel: full mass distributions. Right panel: mass distributions between 30 and 400 amu. With increasing MPM the mass spectra become denser due to increasing Na-doping. Bare Na_j clusters are labelled with the index j in the mass spectrum for 8.8 MPM.

Only the temperature of the Na pickup cell is varied to tune the MPM in Figure S1. The cluster size distribution of the bare ammonia clusters entering the Na pickup zone is kept constant for all mass spectra in this series. Note that the same also holds within the series of mass spectra for small Na-ammonia and Na-dimethyl ether clusters shown in Figures S7 and S9, respectively. However, even though the size distribution of the bare ammonia clusters before the pickup cell is identical, the mass spectra of the Na-doped clusters recorded after Na pickup change with increasing MPM as visible in Figure S1. The overall shape varies and the average cluster size decreases slightly. At MPMs with substantial contribution of bare Na clusters, these Na clusters give rise to the appearance of more pronounced signals at lower masses. Note that similar changes in the shape of the mass spectra with increasing MPM are also observed for small Na-ammonia and Na-dimethyl ether clusters in Figures S7 and S9, respectively. These variations in the mass spectra with MPM are a consequence of cluster heating due to Na-doping. Higher Na-doping (i. e. higher MPM) results in increased heating of the clusters and thus more pronounced cluster evaporation, which explains the shape changes observed in Figure S1 (and Figures S7 and S9). The increased heating at higher MPMs is also reflected in the higher final cluster temperatures T_{cluster} at the location where the clusters are photoionized (see estimated cluster temperatures in Table S1). Section S1.3 explains how these cluster temperatures are calculated. The most pronounced changes in Figure S1 are the sharpened intensity maximum at about 3000 mass units in the mass spectra at 1.2 and 1.3 MPM and the change in shape between 6.2 and 8.8 MPM.

The former feature appears because the size distributions are bimodal. The maxima of the bimodal distributions almost coalesce in the spectra at 1.2 and 1.3 MPM producing a maximum at about 3000 mass units. As the spectra are less congested than at higher MPMs this maximum is also sharper and assumes an almost “peak”-like appearance. In this context it is worth mentioning that such a “peak” cannot indicate a special species, i.e. a magic cluster size with a very distinct geometry. In contrast to the situation in metallic clusters, cluster sizes with distinct geometries do not exist for molecular nanosolution. Note also that the appearance of the “peak”-like signal is not accompanied by any significant change in the photoelectron spectra (Figure 1, main text).

An analysis of the mass spectra reveals that the average size of the Na-ammonia clusters does not change much between 6.2 and 8.8 MPM. But even changes of the average size by a factor of ten would not change the PES significantly. This is clearly borne out by the comparison of Figures 1 and S6: For large Na-ammonia clusters below 8.8 MPM, B_{solv} is virtually identical to the corresponding band in the PES of small $\text{Na}_m(\text{NH}_3)_n$ clusters. The shape of the mass spectra of large NH_3 -ammonia clusters between 6.2 and 8.8 MPM also vary as a consequence of the increased abundance of bare Na-doped clusters in the lower mass range. As explained above, however, bare Na clusters cannot contribute to B_{solv} and thus not to the change of the photoelectron spectrum observed at 8.8 MPM in Figure 1. Similar variations with increasing MPM are observed in the mass spectra of small Na-ammonia and of Na-

dimethyl ether clusters (Figures S7 and S9, respectively). But as the corresponding PES (Figures S6 and S8, respectively) show, such variations in the mass spectra have no significant influence on the position or shape of B_{solv} . We conclude that variations in the mass spectra as observed in Figures S1, S7, and S9 do not significantly affect the corresponding photoelectron spectra so that they can be excluded as a cause for the change in the photoelectron spectrum observed at 8.8 MPM in Figure 1.

S1.2 Determination of the average MPM

Figure S2 shows the **average** MPM as a function of the temperature T in the Na pickup cell. The closed circles indicate the eight different measurements (see Figure S1 and Figure 1 in the main text). The dashed lines indicate the estimated concentration range. For the 8.8 MPM measurement, for example, we estimate the MPM to lie between 6.5 and 10.9. (The definition of MPM is: $\text{MPM} = [\text{moles of metal} / (\text{moles of metal} + \text{moles of solvent molecules}) * 100]$.)

The values for the average MPM are determined as follows: For each temperature T of the Na pickup cell, individual probabilities for the collision of a $(\text{NH}_3)_n$ cluster with k Na atoms ($k = 0, 1, 2, 3, \dots$) are calculated with a Poisson model assuming hard sphere capture cross sections and sticking efficiencies of 1 (see refs.^[1] for details). This results in an average number of Na atoms for each solvent cluster size $(\text{NH}_3)_n$. Examples for the average number of Na atoms as a function of the solvent cluster size n are shown in Figure S3 for three of the eight Na pickup cell temperatures T at which we have performed experiments. The average MPM (Figure S2) for each temperature T is then determined by weighting the contribution of the different cluster sizes according to their abundance in the mass spectrum under single doping conditions.

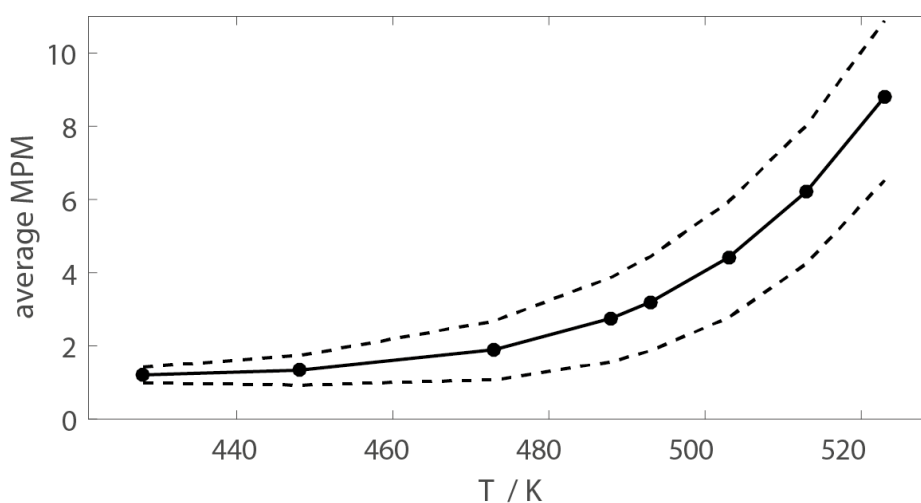


Figure S2: Average MPM as a function of the temperature T of the Na pickup cell. The closed circles correspond to the eight different measurements shown in Figures S1 and 1.

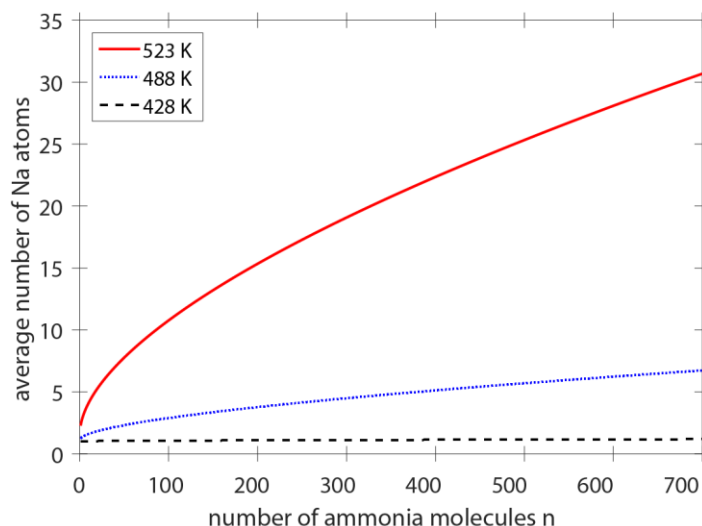


Figure S3: Average number of Na atoms as a function of the solvent cluster size n for three different temperatures T of the Na pickup cell.

S1.3 Cluster Temperature

Neat ammonia clusters are formed in a supersonic expansion ~ 2 cm upstream from a skimmer that separates the nozzle from the Na pickup chamber. Right after the skimmer, the ammonia clusters enter the Na pickup zone, which consists of the actual Na pickup cell and the two effusive Na vapour beams emanating from its entrance and exit holes, respectively.^[1c, 5] The Na-ammonia clusters are ionized directly after the Na pickup cell in the effusive Na beam, without any skimmers between the exit of the pickup cell and the point of ionization. The wavelength (266 nm) of the ionizing laser is chosen such that free Na atoms cannot be ionized.

Evaporative cooling is treated explicitly along the whole range of travel between the nozzle and the point of ionization following the approach described in ref.^[6]. As soon as the solid ammonia clusters enter the pickup zone, they are heated through the collision energy and the energy of solvation of the Na atoms that are picked up. If the doping (MPM) is high enough the Na-ammonia clusters melt so that the final cluster temperature T_{cluster} exceeds the melting temperature. For lower MPMs, T_{cluster} lies below or at the melting point. To estimate T_{cluster} as a function of the average MPM, we use the following parameters. The temperature of the clusters at the exit of the supersonic nozzle is set to 150 K in accordance with ref.^[7]. This value can be varied over a wide range without significantly affecting the final cluster temperature. The reason is the evaporative cooling right after the nozzle which leads to approximately the same temperature at the entrance (skimmer) to the Na pickup zone. The enthalpies of formation, the heat capacities and the vapour pressure curves for liquid and solid ammonia, which are required to describe the evaporative cooling, are taken from refs.^[8]. For lack of corresponding data for Na-ammonia solutions, we have used the pure ammonia parameters also for Na-ammonia clusters. The uptake coefficients for ammonia and Na-ammonia solutions are not known. We have approximated the

value for ammonia by the corresponding value for water ice at its freezing point taken from ref.^[9]. For Na-ammonia solutions, we have assumed a linear dependence of the uptake coefficient on the mole fraction of ammonia modelled after the corresponding data for ice solutions in refs.^[9]. This approximation is expected to be an upper bound to the evaporation rate. To describe the heating by Na uptake, we use an average collision energy per Na atom of 0.17 eV^[1a, 1b], a solvation energy per gaseous Na atom of ~ -1.25 eV from ab initio calculations, and an enthalpy of fusion of $5.8 \cdot 10^{-2}$ eV.^[8c] The melting point of Na-ammonia solutions is not accurately known. Estimates lie between 160 and 190 K.^[10] The upper value of 190 K coincides with a simple estimate of the freezing point depression for a 10 MPM solution. We have used this value in our calculations. The resulting final cluster temperatures T_{cluster} are given in Table S1.

Table S1: Final cluster temperatures T_{cluster} as a function of the average MPM for the data in Figures 1 and S1.

MPM	1.2	1.3	1.9	2.8	3.2	4.4	6.2	8.8
$T_{\text{cluster}} / \text{K}$	169	170	176	183	186	190	190	202

S2 Photoelectron Images

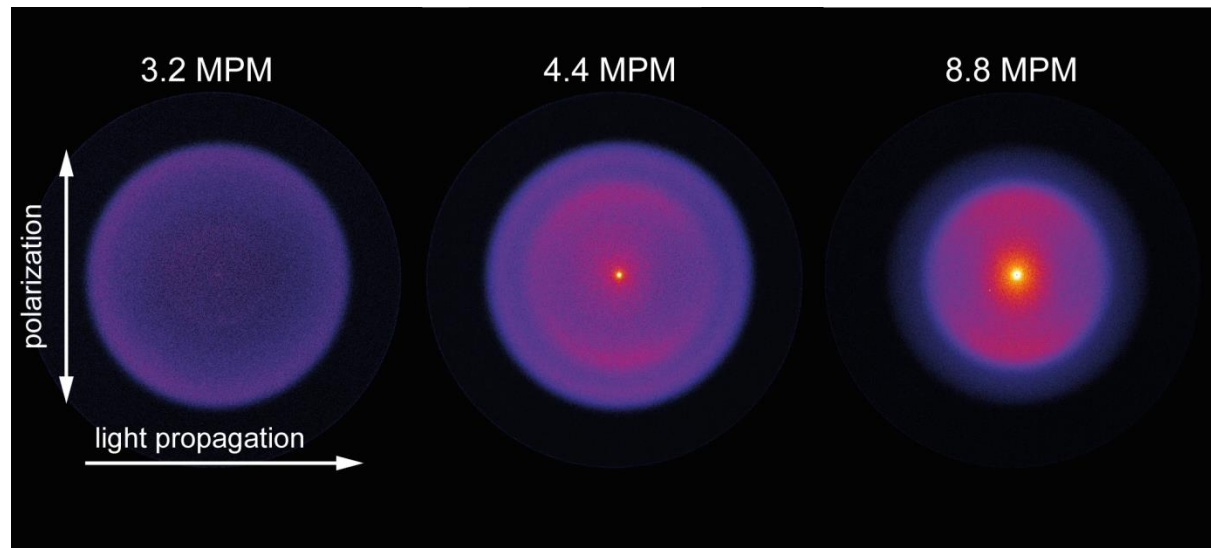


Figure S4: Representative raw photoelectron images^[1c, 11] for 3.2 MPM (non-metallic), 4.4 MPM (non-metallic), and 8.8 MPM (metal-like) are shown. The electron intensity increases from blue to red to yellow. The corresponding PES are shown in Figure 1 in the main text.

S3 Ab initio Calculations

Optimized structures of $\text{Na}(\text{NH}_3)_n$ and $\text{Na}_2(\text{NH}_3)_n$ clusters were calculated with the Gaussian program package^[12] for up to $n = 30$ solvent molecules using the dispersion corrected ωB97XD density functional with a 6-31+G* basis set. For $\text{Na}(\text{NH}_3)_n$ with $n \leq 3$, the results were checked against higher levels of theory (2nd order Møller-Plesset perturbation theory with up to quadruple- ζ correlation consistent basis sets) to confirm that this approach yields reliable equilibrium geometries and an acceptable quantitative description of the balance between solvent-solvent, Na-solvent, and Na^+ -solvent interaction for clusters up to $n = 3$.^[11] Ionic excited states were calculated with TD-DFT. We would like to remark that calculations for small ($n \lesssim 30$) doubly doped clusters can only provide a rough guide to the situation in multiple doped nanoclusters.

Individual electron binding energies (eBE) were determined by subtracting the energy of the neutral cluster from the energy of the ionic cluster with the same geometry, and then referencing to the eBE of free Na. Figure S5 contains the eBEs to the ionic ground state of $\text{Na}_2(\text{NH}_3)_n$ from Figure 2 in the main text together with eBEs for excitations from the neutral ground state to excited ionic states of $\text{Na}_2(\text{NH}_3)_n$ clusters and eBEs of singly Na-doped clusters ($\text{Na}(\text{NH}_3)_n$ (blue crosses in Figure S5).^[11] The Na in the singly-doped clusters is internally solvated, which results in eBEs that coincide with those of $\text{Na}_2(\text{NH}_3)_n$ where both Na atoms are internally solvated (eBE_{solv}, black triangles, green diamonds) (see Figure S5 and Figure 2 in the main text). The internally solvated case shows two classes that mainly differ in the Na-Na distance. The triangles correspond to structures with a Na-Na distance around 3 Å while the Na-Na distance for the diamonds are typically larger than ~7 Å. Both Na atoms contribute to the doubly occupied HOMO of the singlet state. We also find a second structural motif for the $\text{Na}_2(\text{NH}_3)_n$ clusters in singlet states with one of the Na atoms bound to the surface (eBE_{surf}, red squares). The doubly occupied HOMO (essentially 3s) is located at the surface-bound Na atom. Most of the energies of $\text{Na}_2(\text{NH}_3)_n$ structures with $n \geq 20$ lie within less than 0.1-0.2 eV, which means that under our experimental conditions many different structures are likely to contribute to the PES. Figure S5 also reveals that eBEs to the lower excited ionic states (open black circles with the lowest eBEs) lie close to the eBEs to the ionic ground state so that contributions from excited ionic states to the band B_{surf} cannot be excluded. We have also calculated energies and eBEs for representative structures of the lowest triplet state of $\text{Na}_2(\text{NH}_3)_n$ (not shown in Figure S5). Again, typical energy differences and differences in eBE indicate that contributions from triplet states to the PES cannot be excluded.

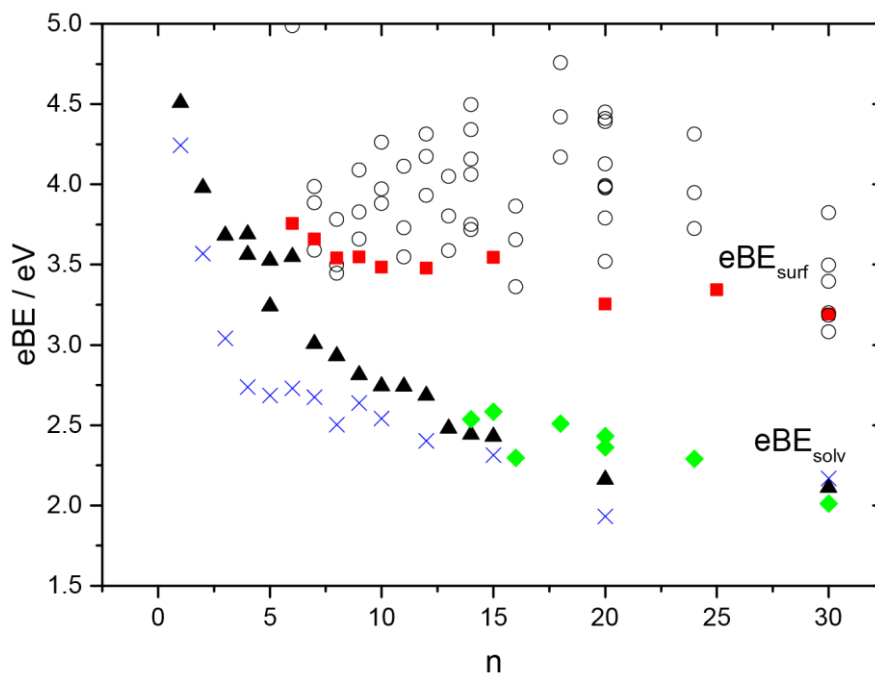


Figure S5: Calculated electron binding energies as a function of cluster size for singly-doped $\text{Na}(\text{NH}_3)_n$ (blue crosses) and for excitations to the ionic ground states of doubly-doped $\text{Na}_2(\text{NH}_3)_n$ (red squares, black triangles, and green diamonds) and to the excited ionic states of $\text{Na}_2(\text{NH}_3)_n$ (open black circle).

S4 Photoelectron Spectra and Size Distributions of Small Na-Ammonia Clusters

Figures S6 and S7 show the photoelectron spectra and the mass spectra of small $\text{Na}_m(\text{NH}_3)_n$ clusters. The average and maximum number of NH_3 solvent molecules are ~ 20 and ~ 80 , corresponding to average and maximum cluster diameters of 1.1 nm and 1.8 nm, respectively.

The appearance of B_{solv} does not undergo any sudden change as a function of MPM (Figure S6) in contrast to the behaviour of large clusters in Figure 1 in the main text. These clusters are likely too small to show a phase transition, even at very high MPM. The features labelled with an asterisk in the PES in Figure S6 arise from very small singly doped $\text{Na}(\text{NH}_3)_n$ clusters with $n \leq 3$ ^[11] formed in high abundance by cluster evaporation in particular at the higher MPMs (see mass spectra in Figure S7). The anisotropy parameter of B_{solv} is $\beta_{\text{solv}} = 0.32 \pm 0.10$ and the anisotropy parameter of B_{surf} is $\beta_{\text{surf}} = 0.54 \pm 0.10$ (Figure S6). This is consistent with the assignment of B_{solv} to internally solvated Na atoms and the assignment of B_{surf} to surface-bound Na atoms. The higher values of the β -parameters for the small clusters compared with the large clusters (Table 1 in the main text) is consistent with less scattering in small clusters.

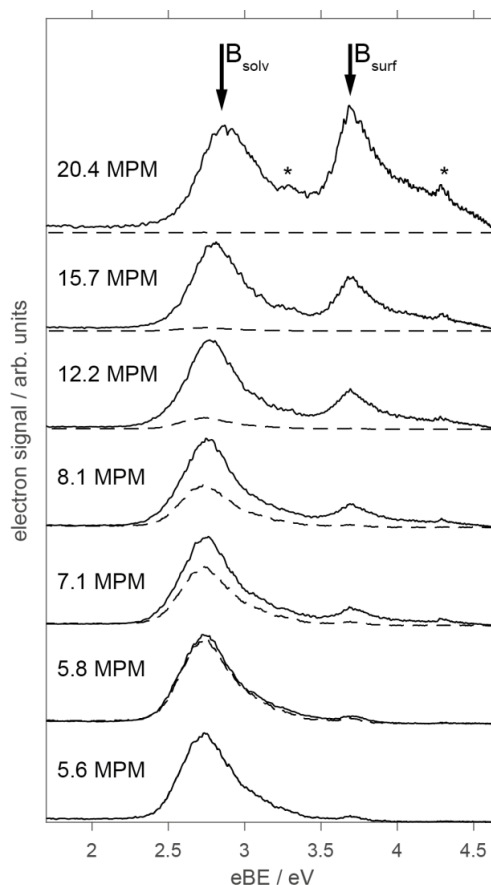


Figure S6: Photoelectron spectra of small $\text{Na}_m(\text{NH}_3)_n$ clusters as a function of the MPM. B_{solv} and B_{surf} indicate structures with internally solvated Na atoms and surface-bound Na atoms, respectively. The dashed lines indicate the contribution of singly Na-doped clusters to the PES and the asterisks point out features arising from very small $\text{Na}(\text{NH}_3)_n$ clusters with $n \leq 3$.

The mass spectra in Figure S7 show similar changes in the shape with increasing MPM as the mass spectra for large Na-ammonia clusters and Na-dimethyl ether clusters in Figures S1 and S9, respectively. As explained in section S1, this is caused by different cluster heating at different MPM, but has no influence on B_{solv} in the corresponding photoelectron spectra in Figure S6. We have also recorded photoelectron spectra (not shown) for size distributions with average sizes between 20 (small clusters) and 200 (large clusters). Below an average size of ~ 100 , we could not find any indications for a TMS.

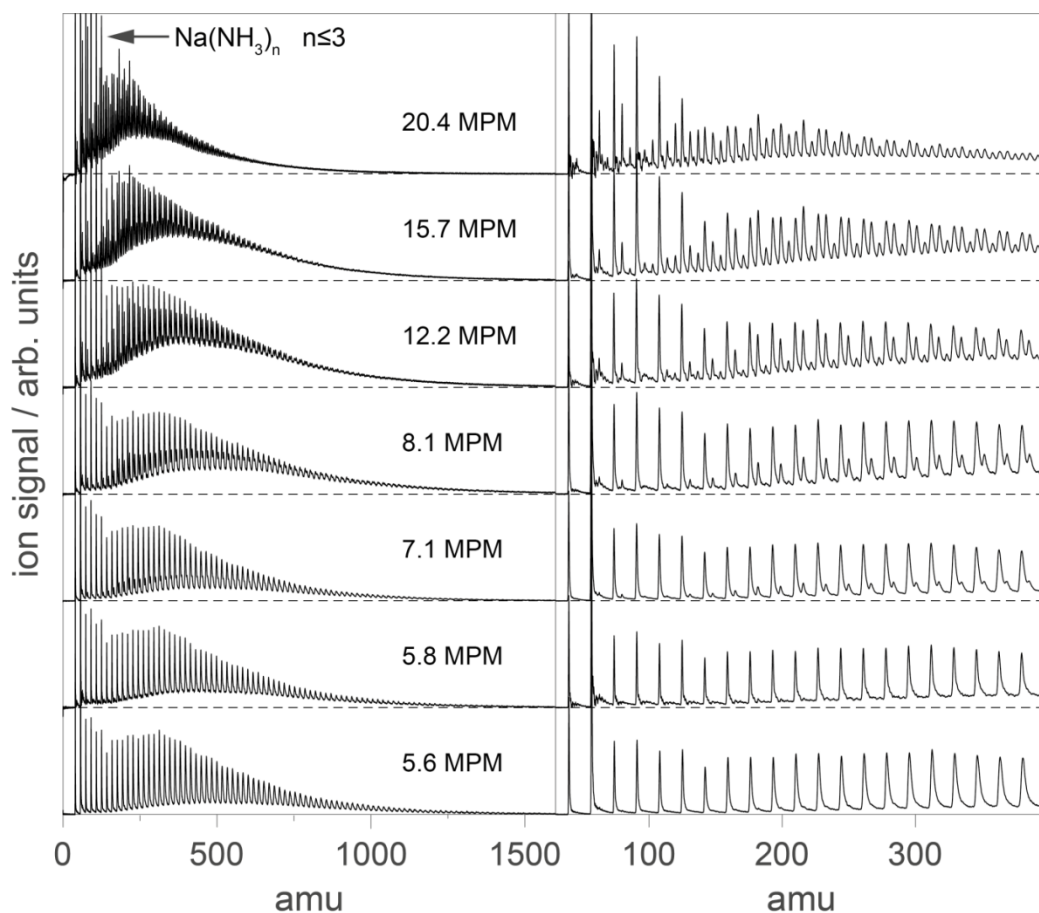


Figure S7: Mass spectra of small $\text{Na}_m(\text{NH}_3)_n$ clusters. Left panel: full mass distributions. Note that the very strong signals of the $\text{Na}_m(\text{NH}_3)_n$ clusters with $n \leq 3$ are cut in the figure. Right panel: mass distributions between 30 and 400 amu. With increasing MPM the mass spectra become denser because of the higher Na-doping.

S5 Photoelectron Spectra and Size Distributions of Na-Dimethyl Ether Clusters

We have recently reported solvation studies of Na in liquid bulk dimethyl ether (see Supporting Information, section 3 in ref.^[11]). These studies reveal that Na does not dissolve in any substantial amount in liquid dimethyl ether at temperatures between 195 K and the boiling point of dimethyl ether (249 K). (The melting point of DME is ~ 132 K.) In contrast to Na-ammonia bulk solutions, metallic Na-dimethyl ether bulk solution should thus not exist and consequently a TMS should not be observed. Therefore, one expects that the photoelectron spectra of Na-dimethyl ether clusters recorded as a function of the MPM should also not show the spectral change observed for the Na-ammonia clusters at 8.8 MPM in Figure 1 in the main text. For this purpose, we have studied many different Na-dimethyl ether clusters with average cluster diameters up to ~ 3.4 nm and MPMs up to ~ 30 . We observe very similar photoelectron spectra at all conditions (Figure S8). Over the range of conditions investigated, none shows any change in B_{solv} comparable to the one observed at 8.8 MPM (Figure 1, main text).

Figures S8 and S9 show one example for dimethyl ether clusters with masses similar to those of the ammonia clusters in Figures 1 and S1.

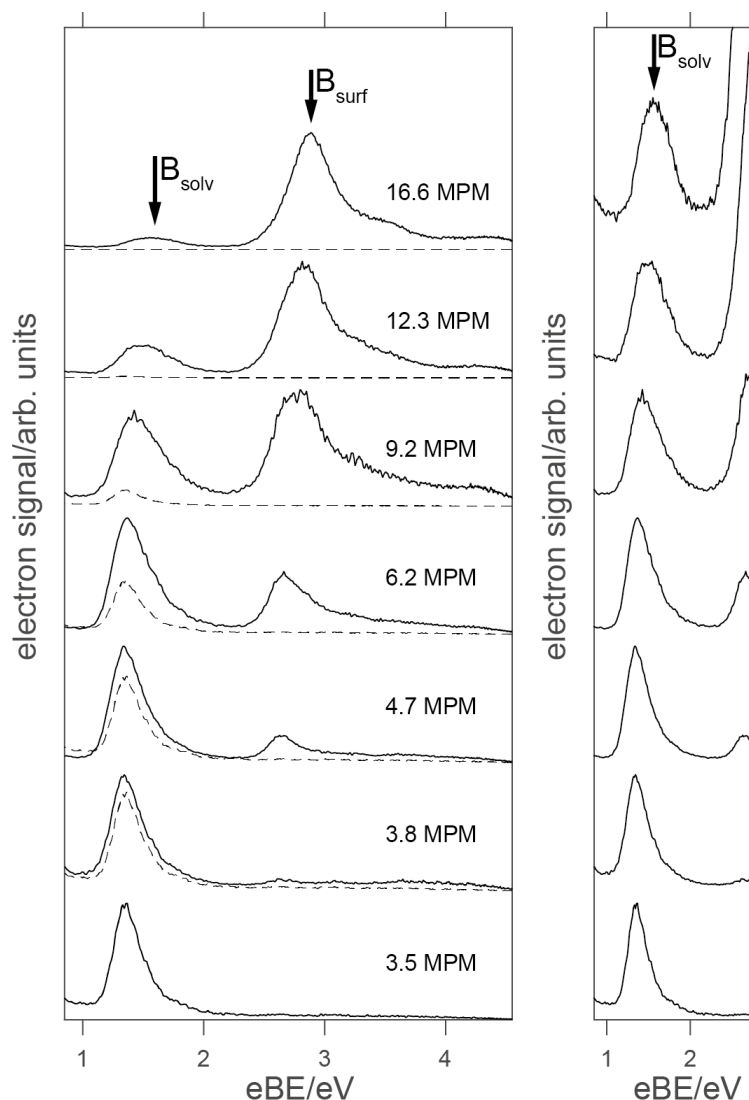


Figure S8: Photoelectron spectra of $\text{Na}_m(\text{CD}_3\text{OCD}_3)_n$ clusters as a function of the MPM. Left: Full range. B_{solv} and B_{surf} indicate structures with internally solvated Na atoms and surface-bound Na atoms, respectively. The dashed lines indicate the contribution of singly Na-doped clusters to the PES. Right: Expanded view around B_{solv} . All spectra are scaled to the band maximum.

The photoelectron spectra in Figure S8 consist of the two bands B_{solv} and B_{surf} , which can be assigned to internally solvated and surface-bound Na atoms, respectively, as for the Na-ammonia clusters. But in contrast to the Na-ammonia clusters, the intensity of B_{solv} simply decreases with increasing MPM until the band almost disappears without showing any significant change in its appearance. There is no shift of PET_{solv} to higher values nor any formation of a plateau comparable to that observed at 8.8 MPM in Figure 1. The same behaviour is also found for Na-dimethyl ether clusters of smaller and larger average sizes (not shown). This observation is consistent with the expectation that a TMS does not occur in Na-dimethyl ether

solutions, and implies that the change in B_{solv} observed at 8.8 MPM in Figure 1 is specific to large Na-ammonia clusters.

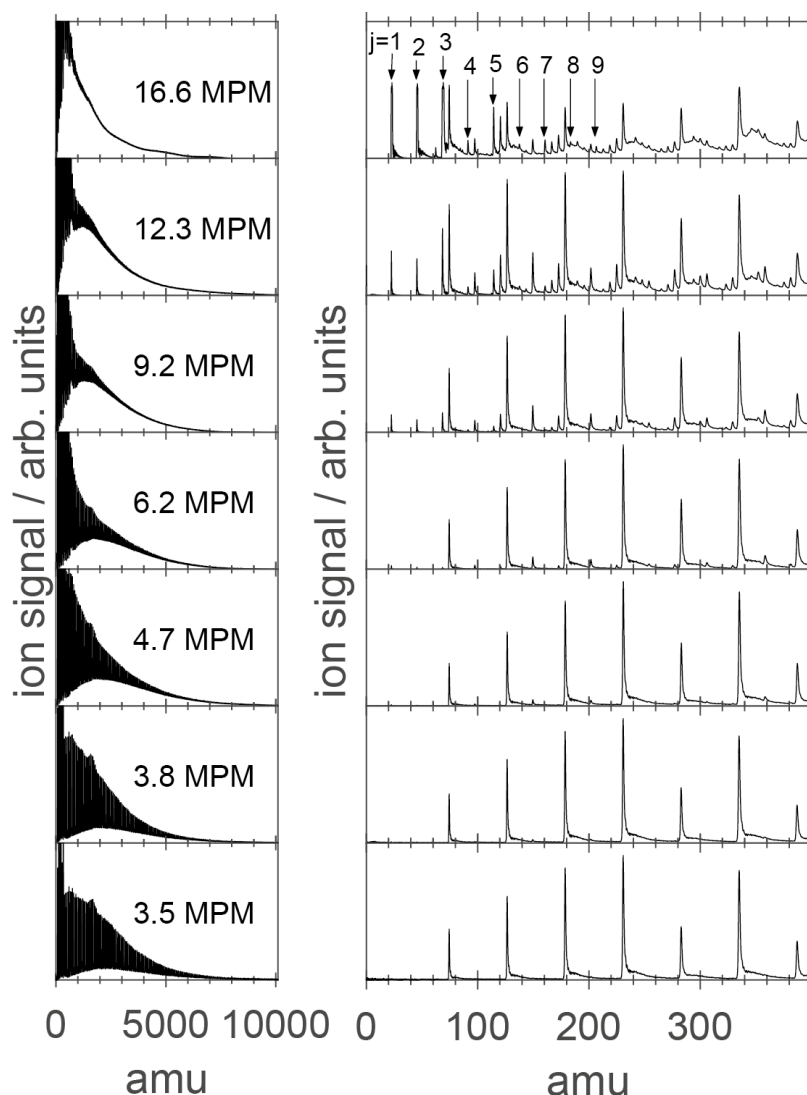


Figure S9: Mass spectra of $\text{Na}_m(\text{CD}_3\text{OCD}_3)_n$ clusters. Left panel: full mass distributions. Note that the strong signals at low masses are cut in the figure. Right panel: mass distributions between 30 and 400 amu. With increasing MPM, the mass spectra become denser due to increasing Na-doping. Bare Na_j clusters are labelled with the index j in the mass spectrum for 16.6 MPM.

The mass spectra in Figure S9 show similar variations in shape with increasing MPM as the mass spectra for large Na-ammonia clusters and small Na-ammonia clusters in Figures S1 and S7, respectively. As explained in Section S1, this is caused by different cluster heating at different MPMs, but has no influence on B_{solv} in the photoelectron spectrum (Figure S8). We estimate similar cluster temperatures as a function of the MPM for Na-dimethyl ether clusters as for the Na-ammonia clusters (see Section 1.3). Bare Na-clusters are clearly visible above about ~ 6.2 MPM in Figure S9. Na_j clusters up to $j=9$ are again labelled with arrows in the 16.6 MPM spectrum. Bare Na clusters with larger j are difficult to distinguish from Na-doped dimethyl ether cluster and are therefore not assigned in Figure S9. The signals of the

Na_j clusters with j=1,2, and 3 at 16.6 MPM are saturated and do not represent true signal heights.

S6 References

- [1] a) B. L. Yoder, J. H. Litman, P. W. Forysinski, J. L. Corbett, R. Signorell, *J. Phys. Chem. Lett.* **2011**, *2*, 2623-2628; b) B. Schläppi, J. J. Ferreiro, J. H. Litman, R. Signorell, *Int. J. Mass Spectrom.* **2014**, *372*, 13-21; c) B. L. Yoder, A. H. C. West, B. Schläppi, E. Chasovskikh, R. Signorell, *J. Chem. Phys.* **2013**, *138*, 044202.
- [2] M. M. Kappes, M. Schär, U. Röthlisberger, C. Yerezian, E. Schumacher, *Chem. Phys. Lett.* **1988**, *143*, 251-258.
- [3] A. Herrmann, S. Leutwyler, E. Schumacher, L. Wöste, *Helv. Chim. Acta* **1978**, *61*, 453-487.
- [4] C. Steinbach, U. Buck, *Phys. Chem. Chem. Phys.* **2005**, *7*, 986-990.
- [5] A. H. C. West, B. L. Yoder, R. Signorell, *J. Phys. Chem. A* **2013**, *117*, 13326-13335.
- [6] J. D. Smith, C. D. Cappa, W. S. Drisdell, R. C. Cohen, R. J. Saykally, *J. Am. Chem. Soc.* **2006**, *128*, 12892-12898.
- [7] N. Gimelshein, S. Gimelshein, C. C. Pradzynski, T. Zeuch, U. Buck, *J. Chem. Phys.* **2015**, *142*, 244305.
- [8] a) <http://webbook.nist.gov>; b) V. A. Popov, V. G. Manzhelii, M. I. Bagatskii, *J. Low Temp. Phys.* **1971**, *5*, 427-433; c) W. M. Haynes, *CRC handbook of chemistry and physics: a ready-reference book of chemical and physical data*, CRC Press, Boca Raton, **2009**.
- [9] C. Delval, B. Fluckiger, M. J. Rossi, *Atmos. Chem. Phys.* **2003**, *3*, 1131-1145.
- [10] O. Ruff, J. Zedner, *Ber. Dtsch. Chem. Ges.* **1908**, *41*, 1948-1960.
- [11] A. H. C. West, B. L. Yoder, D. Luckhaus, C.-M. Saak, M. Doppelbauer, R. Signorell, *J. Phys. Chem. Lett.* **2015**, *6*, 1487-1492.
- [12] M. J. Frisch, G. W. Trucks, H. B. Schlegel, G. E. Scuseria, M. A. Robb, J. R. Cheeseman, G. Scalmani, V. Barone, B. Mennucci, G. A. Petersson, H. Nakatsuji, M. Caricato, X. Li, H. P. Hratchian, A. F. Izmaylov, J. Bloino, G. Zheng, J. L. Sonnenberg, M. Hada, M. Ehara, K. Toyota, R. Fukuda, J. Hasegawa, M. Ishida, T. Nakajima, Y. Honda, O. Kitao, H. Nakai, T. Vreven, J. A. Montgomery Jr., J. E. Peralta, F. Ogliaro, M. J. Bearpark, J. Heyd, E. N. Brothers, K. N. Kudin, V. N. Staroverov, R. Kobayashi, J. Normand, K. Raghavachari, A. P. Rendell, J. C. Burant, S. S. Iyengar, J. Tomasi, M. Cossi, N. Rega, N. J. Millam, M. Klene, J. E. Knox, J. B. Cross, V. Bakken, C. Adamo, J. Jaramillo, R. Gomperts, R. E. Stratmann, O. Yazyev, A. J. Austin, R. Cammi, C. Pomelli, J. W. Ochterski, R. L. Martin, K. Morokuma, V. G. Zakrzewski, G. A. Voth, P. Salvador, J. J. Dannenberg, S. Dapprich, A. D. Daniels, Ö. Farkas, J. B. Foresman, J. V. Ortiz, J. Cioslowski, D. J. Fox, Gaussian, Inc., Wallingford, CT, USA, **2009**.